Fractal analysis of degenerate spiral trajectories of a class of ordinary differential equations

HUZAK, Renato; Vlah, Domagoj; Zubrinic, Darko & Zupanovic, Vesna (2022) Fractal analysis of degenerate spiral trajectories of a class of ordinary differential equations. In: Applied mathematics and computation, 438 (Art N° 127569).

DOI: 10.1016/j.amc.2022.127569
Handle: http://hdl.handle.net/1942/38722

Fractal analysis of degenerate spiral trajectories of a class of ordinary differential equations

Renato Huzak[b], Domagoj Vlah[a,*], Darko Žubrinić[a], Vesna Županović[a]

[a] *University of Zagreb, Faculty of Electrical Engineering and Computing, Department of Applied Mathematics, Unska 3, 10000 Zagreb, Croatia*
[b] *Hasselt University, Campus Diepenbeek, Agoralaan Gebouw D, 3590 Diepenbeek, Belgium*

Abstract

In this paper we initiate the study of the Minkowski dimension, also called the box dimension, of degenerate spiral trajectories of a class of ordinary differential equations. A class of singularities of focus type with two zero eigenvalues (nilpotent or more degenerate) has been studied. We find the box dimension of a polynomial degenerate focus of type (n, n) by exploiting the well-known fractal results for α-power spirals. In the general (m, n) case, we formulate a conjecture about the box dimension of a degenerate focus using numerical experiments. Further, we reduce the fractal analysis of planar nilpotent contact points to the study of the box dimension of a slow-fast spiral generated by their "entry-exit" function. There exists a bijective correspondence between the box dimension of the slow-fast spirals and the codimension of contact points. We also construct a three-dimensional vector field that contains a degenerate spiral, called an elliptical power spiral, as a trajectory.

Keywords: box dimension (Minkowski dimension), degenerate spiral trajectories, geometric chirps, turning points

*Corresponding author.
Email addresses: renato.huzak@uhasselt.be (Renato Huzak), domagoj.vlah@fer.hr (Domagoj Vlah), darko.zubrinic@fer.hr (Darko Žubrinić), vesna.zupanovic@fer.hr (Vesna Županović)

Preprint submitted to Applied Mathematics and Computation

1. Introduction

A fractal-dimensional analysis of the weak focus of a planar vector field $(-y+\dots)\frac{\partial}{\partial x}+(x+\dots)\frac{\partial}{\partial y}$ has been completed in [30, 32] using a box dimension approach. The box dimension of trajectories spiralling around a weak focus has been computed. Furthermore, an explicit relation between the box dimension and the leading power in the asymptotic expansion of the Poincaré map of the weak focus has been obtained (for more details see [30, 32]). The box dimension of spiral trajectories changes from trivial to nontrivial for parameter values at which some bifurcations occur (Hopf-Takens bifurcations [30], Bogdanov-Takens bifurcations [12, 13], discrete saddle-node and period doubling bifurcations [6, 11], etc.) The quality and the quantity of the objects born in the bifurcation is related to the box dimension of a trajectory at the bifurcation parameter.

Our paper is a natural continuation of [30]. We deal with a class of planar singular points of focus type (we assume that the linear part has both eigenvalues equal to zero) and compute their box dimension. Degenerate spirals near such singular points (hence spirals different from weak focus spirals) appear in complex swirling flows. We cite [2]: "Most naturally occurring spirals are anisotropic, developing in systems with inherent asymmetry, such as elliptical whirlpools forming in a flowing body of water. Another simple example arises in Newtonian mechanics: suppose a weight attached to an elastic band is rotated about an axis parallel to the ground. At high velocities the centripetal force dominates gravity and the orbit is circular. However, if the system is allowed to decelerate, the weight will follow a spiral trajectory that will become increasingly elongated in the vertical direction as the relative contribution of gravitational force grows." (Burrell, [2], p. 1)

We focus on a particular deformation (to be specified later) of $X = -ny^{2n-1}\frac{\partial}{\partial x}+mx^{2m-1}\frac{\partial}{\partial y}$, with $m, n \in \mathbb{N}\setminus\{0\}$ and $m+n > 2$, or $Y = (y-x^{2n})\frac{\partial}{\partial x}$ with $n \in \mathbb{N} \setminus \{0\}$. The vector field X has a center at $(x, y) = (0, 0)$, with $H(x, y) = x^{2m} + y^{2n}$ as a first integral, while Y has the curve of singularities $C = \{y = x^{2n}\}$ and horizontal regular orbits (see Figure 1). We say that a vector field X is degenerate if $m > 1$ and $n > 1$, while in the case $m = 1$ or $n = 1$ the vector field X is said to be nilpotent. The vector field Y has a nilpotent singularity at the origin. The fractal-dimensional analysis of such a deformation is far more difficult than the analysis of weak foci due to absence of "regularity" of spiral trajectories. For example, the r-component of a point on any given spiral near the weak focus, is a decreasing function of

time (see Theorem 5 of [30]). This is not true if we deal with the degenerate or nilpotent case. Moreover, the Poincaré map near the focus of the perturbation of X with $m \neq n$ has two different asymptotics, one along the x-axis and the other one along the y-axis. For some other examples of "irregular" spiral trajectories and the calculation of their box dimensions and Minkowski content see e.g. [2, 18, 20, 24, 27, 26].

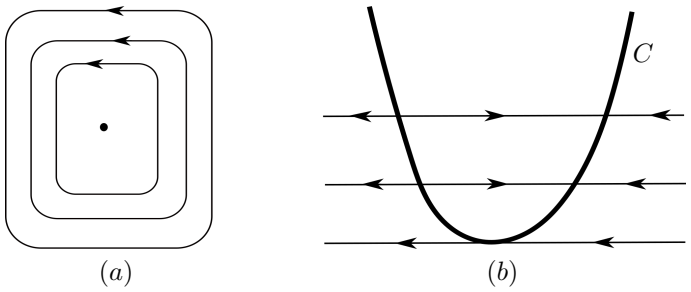

Figure 1: (a) A phase portrait of the vector field X. (b) Dynamics of Y with indication of the curve of singularities C.

In this paper we will often speak about a trajectory "near the origin $(x, y) = (0, 0)$". This stands for its part spiraling around the origin and contained in an open disk centered at the origin.

When $m = n$ and n is odd in X, then we prove the following result (see Theorem 1 in Section 3):

- *Let k be a positive integer. Then any trajectory of the vector field*

$$X_n := X \pm n \left(x^n y^{n-1} (x^{2n} + y^{2n})^k \frac{\partial}{\partial x} + x^{n-1} y^n (x^{2n} + y^{2n})^k \frac{\partial}{\partial y} \right) \quad (1)$$

  near the origin $(x, y) = (0, 0)$ is Minkowski nondegenerate and its box dimension is equal to $2 - \frac{2}{1+2kn}$. If $k = 0$, any trajectory of (1) near the origin is Minkowski measurable and its box dimension is equal to 1.

This has been proved in [30] for $n = 1$ (see also Section 2). When the sign in X_n is negative (resp. positive), we deal with a stable (resp. unstable) focus at the origin. When n is even, then the origin is a center (see Remark 1 in Section 3.1). In the proof of Theorem 1, we construct a bi-Lipschitz map between spiral trajectories of (1) and α-power spirals [28] with a well-known

box dimension. We use the fact that bi-Lipschitz maps preserve the box dimension (see Section 2). Such (degenerate) focus of type (n, n) has the same asymptotic of the Poincaré map in each radial direction (see [23]).

Based on [2] (Remark 4 in Section 4.1) and extensive numerical observations (Section 4.2), in the general case (m and n may be different) we propose the following conjecture:

- *Let k be a positive integer, $m \geq n$ and let m, n be odd. Then any trajectory of*

$$X_{m,n} := X \pm \left(nx^m y^{n-1}(x^{2m} + y^{2n})^k \frac{\partial}{\partial x} + mx^{m-1} y^n (x^{2m} + y^{2n})^k \frac{\partial}{\partial y} \right) \tag{2}$$

near the origin $(x, y) = (0, 0)$ is Minkowski nondegenerate and its box dimension is equal to $2 - \frac{1+\frac{n}{m}}{1+2nk}$.

Note that $X_{n,n} = X_n$. When m is even (resp. n is even), then the system $X_{m,n}$ is invariant under the symmetry $(x, t) \to (-x, -t)$ (resp. $(y, t) \to (-y, -t)$) and has a center at the origin $(x, y) = (0, 0)$ (see Remark 2 in Section 4.1). In the rest of the paper we assume that m and n are odd. A spiral trajectory of (2) cannot be (bi-Lipschitz) mapped onto some regular α-power spiral, for $m \neq n$, due to the presence of different asymptotic expansions of the Poincaré map of (2) depending on the radial direction.

In the case of $k = 0$ in (2) we refer to Theorem 2 in Section 4.1.

We obtain $X_{m,n}$ after applying transformation $F_{m,n} : \mathbb{R}^2 \to \mathbb{R}^2$, defined by

$$(x, y) \mapsto (\bar{x}, \bar{y}) = ((\operatorname{sign} x)|x|^{1/m}, (\operatorname{sign} y)|y|^{1/n}),$$

to X_1, and using multiplication by $mn|\bar{x}|^{m-1}|\bar{y}|^{n-1}$. The map $F_{m,n}$ transforms spiral trajectories of X_1 to spiral trajectories of $X_{m,n}$. It is clear that $F_{m,n}$ is not bi-Lipschitz as $(x, y) \to (0, 0)$, and the box dimension is not necessarily preserved.

The main advantage of working with the model (2) is that in polar coordinates the vector field can be reduced to a Bernoulli or linear differential equation which can be solved. When $m = n$ (resp. $m \neq n$), we use the standard (resp. generalized) polar coordinates. See Section 3.1 (resp. Section 4.1).

If $k = 0$ (resp. $k > 0$) in X_n or $X_{m,n}$, then trajectories near the origin are comparable with exponential spirals (resp. α–power spirals). As it will be

clear in Theorem 1 and Theorem 2, comparability with an α–power spiral is not sufficient to say something about the box dimension of the trajectories near the origin.

The curve of singularities C of Y is divided into a normally attracting part $x > 0$, a normally repelling part $x < 0$ and a nilpotent contact point $(x, y) = (0, 0)$ between them. To study dynamics of a small $O(\epsilon)$-perturbation Y_ϵ of Y ($\epsilon \geq 0$ is a small singular perturbation parameter), one typically uses geometric singular perturbation theory due to Fenichel [8] (Fenichel describes the dynamics of Y_ϵ near normally hyperbolic parts). Near the contact point where the normal hyperbolicity is lost one uses family blow-up (see [4, 21]). The deformation Y_ϵ (often called slow-fast system), with $\epsilon > 0$, may have spiral trajectories (i.e., a focus) near the origin and a natural question arises: How to compute the box dimension of the spiral and does the box dimension tell us something about the type of the contact point (the codimension, cyclicity, etc.)? Instead of computing the box dimension of the spiral at level $\epsilon > 0$, it is more natural to calculate the box dimension of a slow-fast spiral when $\epsilon \to 0$ (see Definition 1 in Section 5). Such slow-fast spiral is a union of a geometric chirp (see [22]) and a part of the curve C near the origin. The geometric chirp is defined using fast and slow subsystems of Y_ϵ and so-called entry-exit relation [1, 3] (see Section 5). We find the box dimension of the slow-fast spiral and establish a bijective correspondence between its box dimension and the codimension of generic or non-generic contact points (see Theorem 3 in Section 5). One of the reasons why it is more convenient to work with slow-fast spirals ($\epsilon = 0$) instead of regular spirals at level $\epsilon > 0$ is that then we don't have to use the family blow-up. We point out that a box dimension approach has already been used in the planar slow-fast setting to study limit cycles configurations Hausdorff close to so-called canard cycles (hence, not contact points). See [14, 17, 15].

As far as we know, the ideas we use to find the box dimension of a degenerate focus (Theorem 1) and the box dimension of a slow-fast spiral (Theorem 3) are original and novel.

Although, for the sake of readability, in this paper we develop techniques for the specific perturbations of X and Y, we believe that similar ideas can be used in a more general framework.

In Section 2 we recall some of the properties of the box dimension that will be often used throughout the paper. Section 3 is devoted to the study of the box dimension of (1) and numerical examples. In Section 4 we find the

box dimension of spiral trajectories of (2) for $k = 0$ and numerically verify the conjecture for different values of m, n and k. Our numerical method in Section 3 and Section 4 is based on a so-called decomposition of ϵ-neighborhoods into tail and nucleus (see [28]). For some other numerical techniques (e.g. differential box counting methods) we refer to [25] and references therein. The fractal analysis of planar nilpotent turning points is given in Section 5. In Section 6 we construct a 3-dimensional vector field having an elliptical power spiral as a trajectory. The conclusion can be found in Section 7.

2. The box dimension and its properties

In this section we briefly recall the notion of box dimension in $\mathbb{R}^N$ (for more details we refer the reader to [7, 22, 28] and references therein). For a bounded set $A \subset \mathbb{R}^N$ we define the *ε-neighbourhood* of A as $A_\varepsilon := \{y \in \mathbb{R}^N : d(y, A) < \varepsilon\}$. By the *lower s-dimensional Minkowski content* of A, for $s \geq 0$, we mean

$$\mathcal{M}_*^s(A) := \liminf_{\varepsilon \to 0} \frac{|A_\varepsilon|}{\varepsilon^{N-s}},$$

and analogously for the *upper s-dimensional Minkowski content* $\mathcal{M}^{*s}(A)$ (we replace $\liminf_{\varepsilon\to 0}$ with $\limsup_{\varepsilon\to 0}$). If $\mathcal{M}^{*s}(A) = \mathcal{M}_*^s(A)$, the common value is called the *s-dimensional Minkowski content of A*, and denoted by $\mathcal{M}^s(A)$. The *lower and upper box dimensions* of A are

$$\underline{\dim}_B A := \inf\{s \geq 0 : \mathcal{M}_*^s(A) = 0\}$$

and analogously $\overline{\dim}_B A := \inf\{s \geq 0 : \mathcal{M}^{*s}(A) = 0\}$. If these two values coincide, we call it simply the *box dimension* of A, and denote it by $\dim_B A$. The upper box dimension is finitely stable, i.e. $\overline{\dim}_B(A_1 \cup A_2) = \max\{\overline{\dim}_B A_1, \overline{\dim}_B A_2\}$, with $A_1, A_2 \subset \mathbb{R}^N$. If $0 < \mathcal{M}_*^d(A) \leq \mathcal{M}^{*d}(A) < \infty$ for some d, then we say that A is *Minkowski nondegenerate*. In this case obviously $d = \dim_B A$. In the case when the lower or upper d-dimensional Minkowski content of A is equal to 0 or ∞, where $d = \dim_B A$, we say that A is *degenerate*. If there exists $\mathcal{M}^d(A)$ for some d such that $\mathcal{M}^d(A) \in (0, \infty)$, then we say that A is *Minkowski measurable*.

Suppose that $F : A \subset \mathbb{R}^N \to \mathbb{R}^M$ is a Lipschitz map. Then

$$\underline{\dim}_B F(A) \leq \underline{\dim}_B A, \ \overline{\dim}_B F(A) \leq \overline{\dim}_B A.$$

If $F : A \subset \mathbb{R}^N \to \mathbb{R}^M$ is a bi-Lipschitz map (i.e., there exist constants $\kappa_1 > 0$ and $\kappa_2 > 0$ such that $\kappa_1 \|x - y\| \leq \|F(x) - F(y)\| \leq \kappa_2 \|x - y\|$, for every $x, y \in A$), then

$$\underline{\dim}_B A = \underline{\dim}_B F(A),\ \overline{\dim}_B A = \overline{\dim}_B F(A).$$

If F is a bi-Lipschitz map and A is Minkowski nondegenerate, then $F(A)$ is Minkowski nondegenerate (see Theorem 4.1 in [31]).

We use the following notation in Section 5. For any two sequences of positive real numbers $(a_l)_{l\in\mathbb{N}}$ and $(b_l)_{l\in\mathbb{N}}$ converging to zero we write $a_l \simeq b_l$, as $l \to \infty$, if there exist positive constants $\tilde{A} < \tilde{B}$ such that $a_l/b_l \in [\tilde{A}, \tilde{B}]$ for all $l \in \mathbb{N}$.

A spiral $r = f(\varphi)$ of focus type is said to be *comparable* with the *α-power spiral* $r = \varphi^{-\alpha}$ if $f(\varphi)/|\varphi|^{-\alpha} \in [\tilde{A}, \tilde{B}]$ for some positive constants $\tilde{A}$ and $\tilde{B}$ and for all $\varphi \in [1, \infty)$ (resp. $\varphi \in (-\infty, -1]$) if the spiral has positive (resp. negative) orientation. Similarly, we say that a spiral $r = f(\varphi)$ of focus type is comparable with the exponential spiral $r = e^{-\beta\varphi}$ if $f(\varphi)/e^{-\beta\varphi} \in [\tilde{A}, \tilde{B}]$ for positive constants $\tilde{A}$ and $\tilde{B}$, a positive (resp. negative) constant β and for all $\varphi \in [0, \infty)$ (resp. $\varphi \in (-\infty, 0]$) if the spiral has positive (resp. negative) orientation. In Section 3.1 (resp. Section 4.1) (r, φ) denotes the standard (resp. generalized) polar coordinates.

Let $\tilde{\Gamma}$ be a trajectory of the vector field

$$-y\frac{\partial}{\partial x} + x\frac{\partial}{\partial y} \pm (x^2 + y^2)^k \left(x\frac{\partial}{\partial x} + y\frac{\partial}{\partial y} \right),\ k \geq 0,$$

near the origin $(x, y) = (0, 0)$, expressed in (standard) polar coordinates as $r = f(\varphi)$. If $k \geq 1$, then $\tilde{\Gamma}$ is comparable with the power spiral $r = \varphi^{-1/2k}$ and $\dim_B \tilde{\Gamma} = \frac{4k}{2k+1}$. If $k = 0$, then $\tilde{\Gamma}$ is comparable with the exponential spiral $r = e^{\pm\varphi}$ and hence $\dim_B \tilde{\Gamma} = 1$. In both cases $\tilde{\Gamma}$ is Minkowski measurable. See Theorem 9 of [30].

3. Box dimension of degenerate focus of type (n, n) and numerical examples

In Section 3.1 we provide a complete study of the box dimension of spiral trajectories of X_n. Section 3.2 is devoted to numerical examples.

3.1. The box dimension of degenerate focus

In this section we prove a result about the box dimension of trajectories of X_n near the origin. We have

Theorem 1. *Let $n \geq 1$ be odd and let $\tilde{\Gamma}$ be a trajectory of X_n, given in (1), near the origin. The following statements are true.*

1. *If $k = 0$, then the spiral $\tilde{\Gamma}$ is comparable with the exponential spiral $r = e^{\pm\varphi/n}$, $\dim_B \tilde{\Gamma} = 1$, and $\tilde{\Gamma}$ is Minkowski measurable.*
2. *If $k > 0$, then the spiral $\tilde{\Gamma}$ is comparable with the power spiral $r = \varphi^{-1/2nk}$,*
$$\dim_B \tilde{\Gamma} = 2 - \frac{2}{1+2kn}, \tag{3}$$
and $\tilde{\Gamma}$ is Minkowski nondegenerate.

Proof. We prefer to work with the system

$$\begin{array}{rcl} \dot{x} &=& -y^{2n-1} \pm x^n y^{n-1}(x^{2n}+y^{2n})^k \\ \dot{y} &=& \quad x^{2n-1} \pm x^{n-1} y^n (x^{2n}+y^{2n})^k, \end{array} \tag{4}$$

obtained by dividing X_n by n (the trajectories near the origin remain unchanged after division by a nowhere zero factor). It suffices to prove Theorem 1 for (4) with the negative sign (stable focus). The case with the positive sign in (4) (unstable focus) can be reduced to the negative sign by reversing the time and applying the coordinate change $(x, y) \to (y, x)$. Thus, in the rest of the proof we focus on the system

$$\begin{array}{rcl} \dot{x} &=& -y^{2n-1} - x^n y^{n-1}(x^{2n}+y^{2n})^k \\ \dot{y} &=& \quad x^{2n-1} - x^{n-1} y^n (x^{2n}+y^{2n})^k, \end{array} \tag{5}$$

with arbitrary but fixed trajectory $\tilde{\Gamma}$ near the origin, given by the initial condition $(x_0, y_0) \neq (0, 0)$. In the polar coordinates $\Theta(r, \varphi) = (r\cos\varphi, r\sin\varphi)$ system (5) becomes

$$\begin{array}{rcl} \dot{r} &=& r^{2n-1}\left(\cos^{2n-1}\varphi\sin\varphi - \sin^{2n-1}\varphi\cos\varphi\right) \\ && -r^{2nk+2n-1}\sin^{n-1}\varphi\cos^{n-1}\varphi\left(\sin^{2n}\varphi+\cos^{2n}\varphi\right)^k \\ \dot{\varphi} &=& r^{2n-2}\left(\sin^{2n}\varphi+\cos^{2n}\varphi\right) \end{array} \tag{6}$$

and the initial condition corresponds to (r_0, φ_0), where $\varphi_0 > 0$. The spiral $\tilde{\Gamma}$ is given in polar coordinates by $r = \tilde{r}(\varphi)$, $\varphi \in [\varphi_0, \infty)$, and $\tilde{r}(\varphi_0) = r_0$. Dividing the first by the second equation in the system (6) we get the equation

$$r'(\varphi) + p(\varphi)r(\varphi) = q(\varphi)r(\varphi)^{2nk+1}, \tag{7}$$

where functions p and q are given by

$$\begin{aligned} p(\varphi) &= \tfrac{\sin^{2n-1}\varphi\cos\varphi-\cos^{2n-1}\varphi\sin\varphi}{\sin^{2n}\varphi+\cos^{2n}\varphi}, \\ q(\varphi) &= -\sin^{n-1}\varphi\cos^{n-1}\varphi\left(\sin^{2n}\varphi+\cos^{2n}\varphi\right)^{k-1}. \end{aligned} \tag{8}$$

When $k = 0$ (resp. $k > 0$), in (7) we deal with a linear equation (resp. Bernoulli differential equation). First we prove Statement 2.

Statement 2. Suppose that $k > 0$. The idea of the proof is to construct a bi-Lipschitz equivalence between $\tilde{\Gamma}$ and some regular α-power spiral [28] (Section 2), with a well known box dimension, and to use the invariance of the box dimension under bi-Lipschitz mappings. We divide the proof into three parts. In the first part we explicitly find the function $\tilde{r}(\varphi)$. In the second part we introduce a radial map which we use to define the bi-Lipschitz map, and the third part is devoted to conclusions.

(a) Finding the spiral $r = \tilde{r}(\varphi)$. Using substitution $z = r^{-2nk}$ we transform (7) to the linear equation

$$-\frac{z'(\varphi)}{2nk} + p(\varphi)z(\varphi) = q(\varphi). \tag{9}$$

We solve (9) using standard techniques and get the solution

$$z(\varphi) = \left(\sin^{2n}\varphi+\cos^{2n}\varphi\right)^{k}(I(\varphi)+C), \tag{10}$$

with $C \in \mathbb{R}$ and

$$I(\varphi) = 2nk\int_0^{\varphi}\frac{\sin^{n-1}\tau\cos^{n-1}\tau}{\sin^{2n}\tau+\cos^{2n}\tau}\,d\tau. \tag{11}$$

Now, we can write the function I from (11) in the form

$$I(\varphi) = K\varphi + P(\varphi), \tag{12}$$

where $K := I(2\pi)/(2\pi)$. Because n is odd, it easily follows that $K > 0$. The function P is given by

$$P(\varphi) = 2nk\int_0^{\varphi-2l\pi}\frac{\sin^{n-1}\tau\cos^{n-1}\tau}{\sin^{2n}\tau+\cos^{2n}\tau}\,d\tau - K(\varphi-2l\pi), \tag{13}$$

where $l = l(\varphi)$ is the largest integer such that $2l\pi \le \varphi$, that is, $l = \lfloor\varphi/(2\pi)\rfloor$, and we used the 2π-periodicity of the subintegral function. It follows from (12) and (13) that P is an analytic and 2π-periodic function, thus bounded.

Now respecting substitution $z = r^{-2nk}$, (10) and (12) we get the solution of (7),

$$r(\varphi) = \left(\sin^{2n}\varphi + \cos^{2n}\varphi\right)^{-\frac{1}{2n}} \left(K\varphi + P(\varphi) + C\right)^{-\frac{1}{2nk}}. \tag{14}$$

Introducing $K_2 := K^{-\frac{1}{2nk}}$, $P_2(\varphi) := P(\varphi)/K$ and $C_2 := C/K$ we rewrite (14) in the form

$$r(\varphi) = K_2 \left(\sin^{2n}\varphi + \cos^{2n}\varphi\right)^{-\frac{1}{2n}} \left(\varphi + P_2(\varphi) + C_2\right)^{-\frac{1}{2nk}}. \tag{15}$$

Thus, $\tilde{r}(\varphi)$ from the definition of $\tilde{\Gamma}$ is given by (15) with C_2 uniquely defined by the initial condition (r_0, φ_0).

(b) Constructing a bi-Lipschitz map S. We take the α-power spiral $\hat{\Gamma}$ from [28], given in polar coordinates by

$$\hat{r}(\varphi) = (\varphi + \hat{C})^{-\alpha}, \tag{16}$$

with $\alpha := \frac{1}{2nk} \in (0,1)$ and $\hat{C} := C_2$. We define a radial map $T : (0,\infty) \times [0, 2\pi) \to (0,\infty) \times [0, 2\pi)$ by

$$T(r, \varphi) := (rH(r, \varphi), \varphi), \tag{17}$$

where the map $H : (0,\infty) \times [0, 2\pi) \to (0,\infty)$ is defined by

$$H(r, \varphi) := K_2 \left(\sin^{2n}\varphi + \cos^{2n}\varphi\right)^{-\frac{1}{2n}} \left(1 + P_2(\varphi) r^{2nk}\right)^{-\frac{1}{2nk}}. \tag{18}$$

The functions T in (17) and H in (18) are chosen in such a way that the composition $S := \Theta \circ T \circ \Theta^{-1} : \mathbb{R}^2 \setminus (0,0) \to \mathbb{R}^2 \setminus (0,0)$ maps $\hat{\Gamma}$ to $\tilde{\Gamma}$, because $P_2(\varphi)$ is a 2π-periodic function.

Also, notice that function H in (18) is bounded and bounded away from zero for r sufficiently small and partial derivatives

$$\begin{aligned}
\frac{\partial H}{\partial r}(r, \varphi) &= -r^{2nk-1} P_2(\varphi)(1 + P_2(\varphi) r^{2nk})^{-1} H(r, \varphi), \\
\frac{\partial H}{\partial \varphi}(r, \varphi) &= \left(\sin^{2n}\varphi + \cos^{2n}\varphi\right)^{-1} (\cos^{2n-1}\varphi \sin\varphi - \cos\varphi \sin^{2n-1}\varphi) H(r, \varphi) \\
&\quad - \frac{1}{2nk} r^{2nk} P_2'(\varphi)(1 + P_2(\varphi) r^{2nk})^{-1} H(r, \varphi)
\end{aligned}$$

exist and are bounded for sufficiently small r, as from (11) and (12) it follows that P_2' is also bounded. Now, all of the conditions of Lemma 1 are satisfied, so we see that function S is a bi-Lipschitz map in a sufficiently small neighborhood of the origin.

(c) Conclusions. As box dimension and Minkowski nondegeneracy is invariant under the bi-Lipschitz mapping (see Section 2), it follows from [28] and Theorem 6.1 in [29] that

$$\dim_B \tilde{\Gamma} = \dim_B \hat{\Gamma} = 2 - \frac{2\alpha}{\alpha+1} = 2 - \frac{2}{1+2kn}, \tag{19}$$

and that $\tilde{\Gamma}$ is Minkowski nondegenerate. Since P_2 is bounded and the term in front of $(\varphi + \cdots)^{-1/2nk}$ in (15) is bounded and bounded away from zero, it is clear that the spiral $\tilde{\Gamma}$ is comparable with the power spiral $r = \varphi^{-1/2nk}$, as $\varphi \to \infty$. This completes the proof of Statement 2.

Statement 1. Let $k = 0$ and let $n \geq 1$ be odd. Using (7) the spiral $\tilde{\Gamma}$ is given by

$$\tilde{r}(\varphi) = Ce^{-\int_0^\varphi (p(\tau)-q(\tau))d\tau} \tag{20}$$

where $C = r_0 e^{\int_0^{\varphi_0} (p(\tau)-q(\tau))d\tau}$ and p and q are given in (8). Since the function p is odd and 2π-periodic, it follows that the integral $\int_0^\varphi p(\tau)d\tau$ is even and 2π-periodic (thus, bounded). On the other hand, the integral $-\int_0^\varphi q(\tau)d\tau$ is equal to the integral given in (11) and can therefore be written as (12), for some new positive constant $K := -\int_0^{2\pi} q(\tau)d\tau/(2\pi)$ and a new 2π-periodic function P (for the exact value of K see the end of the proof of Statement 1). Now, the expression in (20) changes into

$$\tilde{r}(\varphi) = Ce^{-(K\varphi + R(\varphi))} \tag{21}$$

where K is given above and the function R is 2π-periodic and thus bounded. It follows directly from (21) that the spiral $\tilde{\Gamma}$ is comparable with the exponential spiral $r(\varphi) = e^{-K\varphi}$ as $\varphi \to \infty$. Further, the derivative of (20) is equal to

$$\tilde{r}'(\varphi) = (q(\varphi) - p(\varphi))\tilde{r}(\varphi). \tag{22}$$

Using (21), (22) and the fact that p and q are bounded, we get

$$|\tilde{r}'(\varphi)| \leq Me^{-K\varphi}$$

where M is a positive constant. This, together with (21), implies that the length of the spiral $\tilde{\Gamma}$ is finite. Thus, $\dim_B \tilde{\Gamma} = 1$ and $\tilde{\Gamma}$ is Minkowski measurable (see [7] and [28, p. 106]). Notice that the function $\tau \mapsto \frac{1}{n}\arctan(\tan^n \tau)$ is a primitive function of $-q(\tau)$, and this implies that $K = \frac{1}{n}$. This completes the proof of Statement 1. □

Remark 1. *Notice that for n even and $k > 0$ (resp. $k = 0$) it follows from (14) (resp. (20)) that $\tilde{r}(\varphi)$ is 2π-periodic, so the system (5) only has closed periodic trajectories and the fixed point at the origin is of center type.*

In the rest of this section we prove the following lemma used in the proof of Theorem 1.

Lemma 1. *Let $T : (0, \infty) \times \mathbb{R} \to (0, \infty) \times \mathbb{R}$ be a radial map, i.e.,*

$$T(r, \phi) = (rH(r, \phi), \phi),$$

where $H : (0, \infty) \times \mathbb{R} \to (0, \infty)$ is a differentiable function. Suppose that there exist positive real constants r_1, C_1 and C_2 such that

A. $C_1 \leq H(r, \phi) \leq C_2$ for $r \in (0, r_1]$;

B. the partial derivatives $\frac{\partial H}{\partial r}(r, \phi)$ and $\frac{\partial H}{\partial \phi}(r, \phi)$ are bounded for $r \in (0, r_1]$.

Then the map $S : \mathbb{R}^2 \setminus (0, 0) \to \mathbb{R}^2 \setminus (0, 0)$, defined by $S := \Theta \circ T \circ \Theta^{-1}$, where $\Theta(r, \phi) = (r \cos \phi, r \sin \phi)$, has an inverse map S^{-1} and both S and S^{-1} are Lipschitz maps in some punctured neighborhood of the origin.

Proof. It is easy to see that T^{-1} exists and $S^{-1} = \Theta \circ T^{-1} \circ \Theta^{-1}$. To finish the proof we need to see that all of the components of the Jacobian matrices J_S and $J_{S^{-1}}$ are bounded. It is sufficient to prove that S and S^{-1} are Lipschitz maps on the intersection of some punctured neighborhood of the origin and the half-plane $\mathbb{R}^+ \times \mathbb{R}$. As the rotation in the plane is isometry, it follows that S and S^{-1} are Lipschitz maps on the intersection of some punctured neighborhood of the origin and any half-plane given by an arbitrary rotation around the origin of the $\mathbb{R}^+ \times \mathbb{R}$ half-plane. So, by rotating this half-plane around the origin, we can cover a neighborhood of the origin by a finite number of such bi-Lipschitz maps, which proves the Lemma.

We proceed by computing partial derivatives of $S = (S_1, S_2)$ in respect to variables x and y, on a half-plane $\mathbb{R}^+ \times \mathbb{R}$, where Θ^{-1} is explicitly given by

$$\Theta^{-1}(x, y) = \left(\sqrt{x^2 + y^2}, \arctan\left(\frac{y}{x}\right) \right).$$

After meticulous calculation we get

$$\frac{\partial S_1}{\partial x}(x,y) = H(r,\phi)\left(\frac{x}{r}\cos\phi + \frac{y}{r}\sin\phi\right) - \frac{\partial H}{\partial \phi}(r,\phi)\frac{y}{r}\cos\phi + \frac{\partial H}{\partial r}(r,\phi)x\cos\phi, \tag{23}$$

$$\frac{\partial S_1}{\partial y}(x,y) = H(r,\phi)\left(\frac{y}{r}\cos\phi - \frac{x}{r}\sin\phi\right) + \frac{\partial H}{\partial \phi}(r,\phi)\frac{x}{r}\cos\phi + \frac{\partial H}{\partial r}(r,\phi)y\cos\phi, \tag{24}$$

$$\frac{\partial S_2}{\partial x}(x,y) = H(r,\phi)\left(-\frac{y}{r}\cos\phi + \frac{x}{r}\sin\phi\right) - \frac{\partial H}{\partial \phi}(r,\phi)\frac{y}{r}\sin\phi + \frac{\partial H}{\partial r}(r,\phi)x\sin\phi, \tag{25}$$

$$\frac{\partial S_2}{\partial y}(x,y) = H(r,\phi)\left(\frac{x}{r}\cos\phi + \frac{y}{r}\sin\phi\right) + \frac{\partial H}{\partial \phi}(r,\phi)\frac{x}{r}\sin\phi + \frac{\partial H}{\partial r}(r,\phi)y\sin\phi, \tag{26}$$

where we write $r := \sqrt{x^2+y^2}$ and $\phi := \arctan\left(\frac{y}{x}\right)$. As $x, |y| \leq r$, from assumptions A and B we see that terms in expressions (23)–(26) are bounded on the punctured ball $\overline{B}(0;r_1)$, so it follows that all components of the Jacobian J_S are bounded on the punctured ball $\overline{B}(0;r_1)$.

To prove the boundness of $J_{S^{-1}}$, we use the inverse function theorem. It suffices to see that all of the components of the matrix $[J_S]^{-1}$ are bounded. This follows by an elementary computation using well known formula for the inverse of 2×2 matrix and using the fact that

$$\det J_S = H(r,\phi)\left(H(r,\phi) + r\frac{\partial H}{\partial r}(r,\phi)\right)$$

is bounded away from zero for sufficiently small r, using assumptions A and B. □

3.2. Numerical examples

In this section we develop a numerical estimate of the box dimension of trajectories of X_n near the origin. The exact theoretical result has already been proven in the Section 3.1. Here we verify that result numerically and lay ground for later developing numerical verification of conjecture formulated in Section 1.

3.2.1. Numerical estimate of the box dimension

Our goal here is to design a numerical scheme for estimating the box dimension of trajectory $\tilde{\Gamma}$ of X_n, from Theorem 1. We focus on $k > 0$ (the numerical computation of the box dimension of $\tilde{\Gamma}$ when $k = 0$ is similar to the case where $k > 0$). We proceed by dividing trajectory $\tilde{\Gamma}$ to L disjoint parts $\tilde{\Gamma}_j$ such that

$$\tilde{\Gamma}_j := \tilde{\Gamma} \cap \mathcal{K}_j, \quad \forall j,\ 1 \leq j \leq L,$$

where $\mathcal{K}_j$ is an unbounded circular sector between angles $\frac{2(j-1)\pi}{L}$ and $\frac{2j\pi}{L}$.

Next, we estimate the box dimension $\mathcal{D}_j$ of set $\tilde{\Gamma}_j$ for a fixed j. The first step is to estimate the area of ϵ-neighborhood of $\tilde{\Gamma}_j$, which we designate by $|\tilde{\Gamma}_{j,\epsilon}|$. Notice that $\tilde{\Gamma}_j$ is actually a disjoint union of countably many curves of finite length, each curve spanning between two rays:

$$\begin{aligned} R_{j-1} \ \ldots \varphi &= \frac{2(j-1)\pi}{L}, \\ R_j \ \ldots \varphi &= \frac{2j\pi}{L}. \end{aligned}$$

For the purpose of computing $|\tilde{\Gamma}_{j,\epsilon}|$, from (15) it follows that for sufficiently large L and sufficiently close to the origin, we can successfully approximate these countably many curves with parts of circular arcs between rays R_{j-1} and R_j. We denote this set of arcs with $\mathcal{A}_j$, so it approximately holds that $|\tilde{\Gamma}_{j,\epsilon}| \approx |\mathcal{A}_{j,\epsilon}|$, for any small $\epsilon > 0$, that is, the area of ϵ-neighborhood of $\tilde{\Gamma}_j$ is approximately the same as the area of ϵ-neighborhood of $\mathcal{A}_j$. To get the radii of these circular arcs we compute $r(\varphi)$ from (15), by taking $\varphi = \varphi_j + 2i\pi$, for every $i \in \mathbb{N}_0$, where $\varphi_j := \frac{2j\pi}{L}$. By using 2π-periodicity of trigonometric functions and function P_2, from (15) we get

$$r(\varphi) = K_2 \left(\sin^{2n} \varphi_j + \cos^{2n} \varphi_j\right)^{-\frac{1}{2n}} (\varphi_j + 2i\pi + P_2(\varphi_j) + C_2)^{-\frac{1}{2nk}}. \tag{27}$$

Next, we define new constants:

$$\begin{aligned} \alpha &:= \frac{1}{2nk}, \\ K_5 &:= \frac{\varphi_j + P_2(\varphi_j) + C_2}{2\pi}, \\ K_6 &:= K_2 \left(\sin^{2n} \varphi_j + \cos^{2n} \varphi_j\right)^{-\frac{1}{2n}} 2\pi^{-\alpha}, \end{aligned}$$

so we can rewrite (27) as

$$r(\varphi) = K_6(i + K_5)^{-\alpha}. \tag{28}$$

Now each $i \in \mathbb{N}_0$ indexes a single circular arc having the radius equal to

$$r_i := r(\varphi_j + 2i\pi) = K_6(i + K_5)^{-\alpha}. \tag{29}$$

We generalize the approach from [28], where the concept of nucleus and tail part of ϵ-neighborhood was introduced. For a fixed $\epsilon > 0$, we define critical $i_1 = i_1(\epsilon)$ as the smallest integer i such that $r_i - r_{i+1} \leq 2\epsilon$. This critical i_1 divides the tail part from the nucleus part of the ϵ-neighbourhood of the set $\mathcal{A}_j$. The tail part corresponds to ϵ-neighbourhood of all arcs from $\mathcal{A}_j$ having indices $i \leq i_1$. These arcs all have disjoint ϵ-neighbourhoods. On the contrary, the nucleus part corresponds to ϵ-neighbourhood of all arcs from $\mathcal{A}_j$ having indices $i > i_1$. These arcs have overlapping ϵ-neighborhoods.

To proceed, we first solve the equation $r_\beta - r_{\beta+1} = 2\epsilon$, allowing $\beta \geq 0$ to be a real number, and then taking $i_1 := \lceil \beta \rceil$. We rewrite the equation as

$$f(\beta + K_5) - f((\beta + K_5) + 1) = \frac{2\epsilon}{K_6}, \tag{30}$$

where $f(x) = x^{-\alpha}$. As function f is an analytic function for all $x > 0$, and we can make K_5 arbitrarily large by choosing the initial condition close to the origin and ϵ close to 0, we can develop the second term on the left hand side of (30) in Taylor series around point $x_0 = \beta + K_5$. By taking only the first two terms in this Taylor series, we get an approximate form of equation (30),

$$\alpha(\beta + K_5)^{-\alpha-1} \approx \frac{2\epsilon}{K_6}, \tag{31}$$

which can easily be solved. Notice that it is not possible to find solution β of the original equation (30) in closed form. We get the approximate solution β and compute

$$i_1 = \lceil \beta \rceil = \left\lceil \left(\frac{\alpha K_6}{2\epsilon} \right)^{\frac{1}{\alpha+1}} - K_5 \right\rceil. \tag{32}$$

Last, we estimate the area of the tail and nucleus part of $|\mathcal{A}_{j,\epsilon}|$. The sum of this tail and nucleus is then approximately equal to $|\tilde{\Gamma}_{j,\epsilon}|$.

To get the area of the tail part we first have to compute the sum $\mathcal{S}_j := \sum_{i=0}^{i_1} r_i$. As i_1 could be very large and thus impossible for exact summation,

we approximate $\mathcal{S}_j$ using method of the interval test for convergence, where we compute the approximation error to be smaller than $K_6/(K_5)^\alpha$. We can take K_5 to be sufficiently large, as before, so the approximation error can be made arbitrarily small. For sum $\mathcal{S}_j$, we get

$$\mathcal{S}_j \approx K_6 \int_0^{i_1+1} \frac{dt}{(t+K_5)^\alpha} = K_6 \frac{(i_1+1+K_5)^{1-\alpha} - K_5^{1-\alpha}}{1-\alpha}. \tag{33}$$

The area of the tail part is equal to the sum of ϵ-neighborhoods of all circular arcs in the tail part of $\mathcal{A}_j$. We approximate ϵ-neighborhood of every circular arc in tail part arc using the ϵ-neighborhood of a segment having the same length as the arc. As all of this ϵ-neighborhoods are disjoint, we compute the total sum of this ϵ-neighborhoods to be $\mathcal{S}_j(2\pi/L)\cdot 2\epsilon + (i_1+1)\epsilon^2$. On the other hand, the area of the nucleus part is equal to $(r_{i_1})^2\pi/L$. Finally, using (33) we get

$$|\tilde{\Gamma}_{j,\epsilon}| \approx \left(K_6 \frac{(i_1+1+K_5)^{1-\alpha} - K_5^{1-\alpha}}{1-\alpha} \right) \frac{4\pi}{L}\epsilon + (i_1+1)\epsilon^2 + (r_{i_1})^2 \frac{\pi}{L}. \tag{34}$$

We estimate the box dimension of set $\tilde{\Gamma}_j$ using a standard formula from [7],

$$\mathcal{D}_j := \dim_B \tilde{\Gamma}_j = 2 - \lim_{\epsilon\to 0} \frac{\log|\tilde{\Gamma}_{j,\epsilon}|}{\log\epsilon}. \tag{35}$$

Precisely, we approximate $\mathcal{D}_j$ by evaluating (35) for some fixed $\epsilon_0 > 0$, that is very close to zero,

$$\mathcal{D}_j \approx 2 - \frac{\log|\tilde{\Gamma}_{j,\epsilon_0}|}{\log\epsilon_0}. \tag{36}$$

Using the area of the tail and the nucleus part from (34) and substituting to (36), we compute

$$\mathcal{D}_j \approx 2 - \frac{\log\left[\left(K_6 \frac{(i_1+1+K_5)^{1-\alpha} - K_5^{1-\alpha}}{1-\alpha}\right)\frac{4\pi}{L}\epsilon_0 + (i_1+1)\epsilon_0^2 + (r_{i_1})^2\frac{\pi}{L}\right]}{\log\epsilon_0}. \tag{37}$$

Finally, we use estimates $\mathcal{D}_j$ from (36) of the box dimension of $\tilde{\Gamma}_j$ to estimate upper and lower bounds on the box dimension of $\tilde{\Gamma}$. We assume that $\dim_B \tilde{\Gamma}_j$ exists and is approximately equal to previously obtained $\mathcal{D}_j$.

We use monotonicity of the upper and lower box dimension, and also finite stability of the upper box dimension (see [7]) to compute required estimates. For the estimate on the upper bound, we have

$$\overline{\dim}_B\tilde{\Gamma} = \max_{1\le j\le L} \overline{\dim}_B\tilde{\Gamma}_j \approx \max_{1\le j\le L} \mathcal{D}_j. \tag{38}$$

For the lower bound we first see that

$$\mathcal{D}_j \approx \underline{\dim}_B\tilde{\Gamma}_j \le \underline{\dim}_B\tilde{\Gamma}, \quad \forall j,\ 1\le j\le L,$$

from which follows that

$$\max_{1\le j\le L} \mathcal{D}_j \approx \max_{1\le j\le L} \underline{\dim}_B\tilde{\Gamma}_j \le \underline{\dim}_B\tilde{\Gamma}. \tag{39}$$

Using estimates (39) and (38), as $\underline{\dim}_B\tilde{\Gamma} \le \dim_B\tilde{\Gamma} \le \overline{\dim}_B\tilde{\Gamma}$, we finally see that

$$\dim_B\tilde{\Gamma} \approx \max_{1\le j\le L} \mathcal{D}_j. \tag{40}$$

3.2.2. Implementation details and test results

We implemented the algorithm for computing our numerical estimate of the box dimension using Wolfram Mathematica, version 12. See `https://github.com/FRABDYN/DegenerateSpirals` where our code is available for download. All computations have been done symbolically, using exact fractions where appropriate, having essentially infinite numerical precision. The box dimension results were only numericalized in step (37) when computing $\mathcal{D}_j$.

We present numerically computed dimension for different examples having different values of n and k in Table 1. The rest of the comments in this section refer specifically to cases when $k > 0$. Case $k = 0$ is similar. Refer to the Mathematica code for more information.

We used the initial condition values of $r_0 = 1/10$ and $\varphi_0 = 0$, corresponding to the constant C from (10) equal to 100^{nk}. By computing the integral I from (11) we get that constant $K = 2k$. Furthermore, to speed up the calculation we approximate constant K_5 by $C_2/(2\pi)$ as $\varphi_j + P_2(\varphi_j)$ is at least 10^{10} times less than C_2.

For all test cases we decided to use $\epsilon_0 = 10^{-10000}$ and $L = 1000$. Using this values we produced results having high numerical precision compared to the theoretical result from Theorem 1 and computations last no more than few seconds on a modern PC computer. For even higher precision, value of ϵ could be further decreased and L increased, which would increase the computation time.

n	k	theoretical dimension		numerical dimension
3	0	1	1.00000	0.99982
11	0	1	1.00000	0.99986
21	0	1	1.00000	0.99988
3	2	24/13	1.84615	1.84593
3	11	132/67	1.97015	1.96992
11	2	88/45	1.95556	1.95534
11	11	484/243	1.99177	1.99155
21	2	168/85	1.97647	1.97625
21	11	924/463	1.99568	1.99546

Table 1: Theoretical and numerical box dimensions computed for different values of n and k.

4. Box dimension of degenerate focus of type (m, n)

In Section 4.1 we introduce generalized polar coordinates and show that for $k = 0$ the box dimension of spiral trajectories of $X_{m,n}$ is equal to one (Theorem 2). In Section 4.2 we illustrate the method used in Section 4.1 with numerical examples, and (numerically) verify the conjecture formulated in Section 1 for different values of m, n and k.

4.1. Generalized polar coordinates

We study the box dimension of spiral trajectories of $X_{m,n}$–given in (2)–near the origin. We write the system as

$$\begin{aligned} \dot{x} &= -ny^{2n-1} \pm nx^m y^{n-1}(x^{2m} + y^{2n})^k \\ \dot{y} &= \quad mx^{2m-1} \pm mx^{m-1} y^n (x^{2m} + y^{2n})^k. \end{aligned} \tag{41}$$

We introduce (see [9, 10]) the (n, m)–polar coordinates

$$(x, y) = (r^n \mathrm{Cs}(\varphi), r^m \mathrm{Sn}(\varphi))$$

where $\mathrm{Cs}(\varphi)$ and $\mathrm{Sn}(\varphi)$ are a generalization of $\cos\varphi$ and $\sin\varphi$, and satisfy

$$\dot{\mathrm{Cs}}(\varphi) = -n\mathrm{Sn}^{2n-1}(\varphi),\ \dot{\mathrm{Sn}}(\varphi) = m\mathrm{Cs}^{2m-1}(\varphi)$$

and $(\mathrm{Cs}(0), \mathrm{Sn}(0)) = (1, 0)$. Notice that $\mathrm{Cs}^{2m}(\varphi) + \mathrm{Sn}^{2n}(\varphi) = 1$, $\mathrm{Cs}(\varphi)$ (resp. $\mathrm{Sn}(\varphi)$) is even (resp. odd) and both are T-periodic, with

$$T = \frac{2}{mn} \frac{\Gamma(\frac{1}{2m})\Gamma(\frac{1}{2n})}{\Gamma(\frac{1}{2m} + \frac{1}{2n})},$$

where Γ is the gamma function. In these polar coordinates system (41) becomes

$$\frac{dr}{d\varphi} = \pm \mathrm{Sn}^{n-1}(\varphi)\mathrm{Cs}^{m-1}(\varphi) r^{2mnk+1}, \tag{42}$$

upon division of $\dot{r}$ by $\dot{\varphi}$. We use the following simple lemma (see [9]) in the proof of Theorem 2.

Lemma 2. *Let T be the period of the functions $Cs(\varphi)$ and $Sn(\varphi)$. The following statements are true.*

1. *If either m or n is even, then $\int_0^T Sn^{n-1}(\varphi)\, Cs^{m-1}(\varphi) d\varphi = 0$.*
2. *If both m and n are odd, then $\int_0^T Sn^{n-1}(\varphi)\, Cs^{m-1}(\varphi) d\varphi = \frac{2\pi}{mn}$.*

Theorem 2. *Let T be the period of the functions $Cs(\varphi)$ and $Sn(\varphi)$. If both m and n are odd, then the following statements are true for a spiral trajectory $\tilde{\Gamma}$ of (41) near the origin.*

1. *If $k = 0$, then the spiral $\tilde{\Gamma}$ is comparable with the exponential spiral $r = e^{\pm \frac{2\pi}{Tmn}\varphi}$, $\dim_B \tilde{\Gamma} = 1$, and $\tilde{\Gamma}$ is Minkowski measurable.*
2. *If $k > 0$, then spiral $\tilde{\Gamma}$ is comparable with the power spiral $r = \varphi^{-1/2mnk}$.*

Proof. First we prove Statement 1. When $k = 0$, then the spiral $\widetilde{\Gamma}$ is given by

$$\tilde{r}(\varphi) = Ce^{\pm \int_0^\varphi \mathrm{Sn}^{n-1}(\tau)\mathrm{Cs}^{m-1}(\tau) d\tau} \tag{43}$$

where the constant $C > 0$ is uniquely determined by the initial condition on $\tilde{\Gamma}$. We used (42). Now we proceed exactly as in the proof of Theorem 1. We have

$$\int_0^\varphi \mathrm{Sn}^{n-1}(\tau)\mathrm{Cs}^{m-1}(\tau) d\tau = \left(\frac{1}{T} \int_0^T \mathrm{Sn}^{n-1}(\tau)\mathrm{Cs}^{m-1}(\tau) d\tau \right) \varphi + P(\varphi), \tag{44}$$

with

$$P(\varphi) = \int_0^{\varphi - lT} \mathrm{Sn}^{n-1}(\tau)\mathrm{Cs}^{m-1}(\tau) d\tau - \frac{1}{T} \int_0^T \mathrm{Sn}^{n-1}(\tau)\mathrm{Cs}^{m-1}(\tau) d\tau \, (\varphi - lT),$$

where l is the largest integer such that $lT \leq \varphi$, that is, $l = \lfloor \varphi/T \rfloor$ (we use that the integrand function is T-periodic). The function P is bounded and T-periodic. Now, using this, Lemma 2.2, (43) and (44), we have that $\tilde{\Gamma}$ is comparable with the exponential spiral $r = e^{\pm \frac{2\pi}{Tmn}\varphi}$. Since $\mathrm{Cs}(\varphi)$ and $\mathrm{Sn}(\varphi)$ are bounded, the length of $\tilde{\Gamma}$ is finite. This completes the proof of Statement 1.

To prove Statement 2, it suffices to notice that the spiral $\tilde{\Gamma}$ is given by

$$\tilde{r}(\varphi) = \left(\mp 2mnk \int_0^{\varphi} \mathrm{Sn}^{n-1}(\tau)\mathrm{Cs}^{m-1}(\tau)d\tau + C \right)^{-\frac{1}{2mnk}} \tag{45}$$

and to use (44). □

Remark 2. *If either m or n is even, then the first statement of Lemma 2 implies that system (41) has a center at the origin.*

Remark 3. *When $n = m$, then we deal with the (n, n)–polar coordinates $(x, y) = (r^n Cs(\varphi), r^n Sn(\varphi))$. Notice that in Section 3, instead of these generalized polar coordinates, we worked with the standard polar coordinates in which the α–power spirals [28] are expressed. This was important in the proof of Theorem 1 when $k > 0$.*

Remark 4. *In [2] it is proved that the box dimension of the planar elliptical spiral $(x(\varphi), y(\varphi)) = (\varphi^{-p_0}\cos\varphi, \varphi^{-q_0}\sin\varphi)$, $1 < \varphi < \infty$, with $0 < p_0 \leq q_0$ and $p_0 < 1$, is equal to $2 - \frac{p_0+q_0}{1+q_0}$. If we replace $Cs(\varphi)$ and $Sn(\varphi)$ with $\cos\varphi$ and $\sin\varphi$, in the definition of (n, m)–polar coordinates, and (45) with $\tilde{r}(\varphi) = \varphi^{-\frac{1}{2mnk}}$, then we obtain a natural candidate for the box dimension of the spiral $\tilde{\Gamma}$ when $k > 0$ and $m \geq n$, which is equal to $2 - \frac{1+\frac{n}{m}}{1+2nk}$. Note that $p_0 = \frac{1}{2mk}$ and $q_0 = \frac{1}{2nk}$.*

4.2. Numerical verification of Conjecture

Let $m > n$ and $k > 0$. To verify the conjecture formulated in Section 1, we use a method similar to that used in Section 3.2.1. Instead of using the (n, m)–polar coordinates introduced in Section 4.1, from a numerical point of view it is better to express a spiral trajectory $\tilde{\Gamma}$ of (41) in r, φ where $(x, y) = (r^n \cos\varphi, r^m \sin\varphi)$. In this way, we avoid the computation of $\mathrm{Cs}(\varphi)$ and $\mathrm{Sn}(\varphi)$. Like in Section 3.2.1, we numerically compute the box dimension of $\tilde{\Gamma}$ in sectors $\mathcal{K}_j$ ($\mathcal{K}_j$ between $\varphi = \frac{(2(j-1)+1)\pi}{L}$ and $\varphi = \frac{(2j+1)\pi}{L}$, $1 \leq j \leq L$).

We find r_i which has a form similar to (29). This corresponds to circular arcs having the radius equal to R_i where (R, θ) are the standard polar coordinates $(x, y) = (R\cos\theta, R\sin\theta)$. R_i can also be brought into the form (29). The length $\Delta\theta_i$ of the circular arc with the radius R_i can be expressed in terms of r_i and φ_j. Finally, we compute the tail part and the nucleus part, like in Section 3.2.1.

m	n	k	conjectured dimension		numerical dimension
5	3	2	122/65	1.87692	1.87287
11	3	2	272/143	1.90210	1.89615
21	3	2	174/91	1.91209	1.90574
21	11	2	1858/945	1.96614	1.96561
5	3	11	662/335	1.97612	1.97581
11	3	11	1460/737	1.98100	1.98063
21	3	11	930/469	1.98294	1.98255
21	11	11	10174/5103	1.99373	1.99355

Table 2: Conjectured and numerical box dimensions computed for different values of m, n and k.

Similarly as in Section 3.2.2, in Table 2 we present numerically computed dimension for different values of m, n and k. We also include our Mathematica code available for download.

For the initial condition we used again $r_0 = 1/10$ and $\varphi_0 = 0$. For computing the ϵ-neighborhood to approximate limit from (35), we used $\epsilon_0 = 10^{-10000}$ and we divided $\tilde{\Gamma}$ in $L = 1000$ sectors. Using these values we were able to compute dimension to high precision compared to the conjectured result.

5. The box dimension of slow-fast spirals near nilpotent contact points

Notation $n, C, k, \ldots$ that we will use in this section has nothing to do with $n, C, k, \ldots$ used in Sections 3 and 4. We consider a C^∞-smooth family of Liénard slow-fast systems

$$\begin{aligned} \dot{x} &= y - x^{2n} \\ \dot{y} &= \epsilon(a + F(x, \rho)) + O(\epsilon^2) \end{aligned} \tag{46}$$

where $\epsilon \geq 0$ is a (small) singular parameter, $a \sim 0 \in \mathbb{R}$, $\rho \sim 0 \in \mathbb{R}^m$, $n \geq 1$ is an integer, $F(x,\rho)$ and $O(\epsilon^2)$ are C^∞-functions and $F(x,\rho) = -x^{2n-1}+O(x^{2n})$. We denote system (46) by $X_{\epsilon,a,\rho}$. When $\epsilon = 0$, system $X_{\epsilon,a,\rho}$ has a curve of singularities given by $C = \{y - x^{2n} = 0\}$. All the singularities are normally hyperbolic (i.e. precisely one eigenvalue of the linear part of $X_{0,a,\rho}$ at $p \in C$ is zero). An exception is the point $p = (0,0) \in C$ which is a nilpotent singularity (i.e., the normal hyperbolicity at the origin is lost). When $n = 1$ (resp. $n > 1$), we call the origin in $X_{\epsilon,a,\rho}$ a generic (resp. non-generic) contact point (see e.g. [16]). We focus on the fractal analysis of the slow-fast spirals near the contact point (see Definition 1) in both generic and non-generic case. We use the notion of box dimension in two dimensional ambient space and geometric chirps.

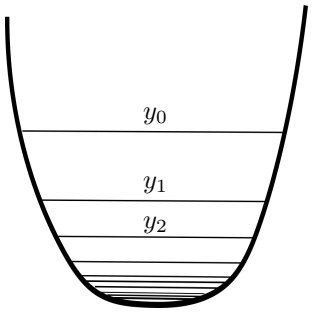

Figure 2: The geometric (δ_1, δ_2)-chirp, with $\delta_1 := \frac{1}{2n}$ and $\delta_2 := \frac{2(k-n)+1}{2n}$, defined near the contact point of $X_{\epsilon,a,\rho}$ with codimension k ($k \geq n$).

We denote by Σ a section inside $\{x = 0\}$, parametrized by $y \geq 0$, $y \sim 0$ ($y = 0$ corresponds to the origin $(x,y) = (0,0)$). We define the slow divergence integral along the attracting part $\{x > 0, x \sim 0\}$ (resp. the repelling part $\{x < 0, x \sim 0\}$) of C:

$$J_-(y,\rho) := \int_{\omega(y)}^{0} \frac{-(2nx^{2n-1})^2 dx}{F(x,\rho)} < 0$$
$$\left(\text{resp. } J_+(y,\rho) := \int_{\alpha(y)}^{0} \frac{-(2nx^{2n-1})^2 dx}{F(x,\rho)} < 0\right)$$

where $(y,\rho) \sim (0,0)$, $y > 0$ and $\omega(y) = y^{\frac{1}{2n}} > 0$ (resp. $\alpha(y) = -y^{\frac{1}{2n}} < 0$) is the ω-limit (resp. α-limit) of the fast horizontal orbit of $X_{0,a,\rho}$ through $y \in \Sigma$. The divergence of $X_{0,a,\rho}$ is given by $-2nx^{2n-1}$ and the slow dynamics along

C is $\frac{dx}{d\tau} = \frac{F(x,\rho)}{2nx^{2n-1}}$ where τ is the slow time. Note that $J_\pm$ are well-defined (i.e. finite) because the leading term of F is x^{2n-1}.

We assume that $(J_- - J_+)(y,0) \neq 0$ for all $y \sim 0$ and $y > 0$. (In the limit $y = 0$, we have $(J_- - J_+)(0,0) = 0$ because $\alpha(0) = \omega(0) = 0$.) If $(J_- - J_+)(y,0) < 0$ for $y \sim 0$ and $y > 0$ (resp. $(J_- - J_+)(y,0) > 0$ for $y \sim 0$ and $y > 0$), then the orbit $\mathcal{O} = \{y_0, y_1, y_2, \dots\}$, defined recursively by

$$J_-(y_{l+1},0) = J_+(y_l,0) \ \text{(resp. } J_-(y_l,0) = J_+(y_{l+1},0)\text{)}, \ l \geq 0, \tag{47}$$

with $y_0 > 0$ small and fixed, is decreasing and converges to zero. This is a simple consequence of the fact that the integrand in $J_\pm$ changes sign as x varies through $x = 0$.

Using the orbit $\mathcal{O}$ we define a geometric chirp near the contact point of $X_{\epsilon,a,\rho}$ (at level $(\epsilon, a, \rho) = (0,0,0)$):

$$\mathcal{U} = \bigcup_{y_l \in \mathcal{O}} U_l \subset \mathbb{R}^2, \quad U_l = (\alpha(y_l), \omega(y_l)) \times \{y_l\}. \tag{48}$$

The geometric chirp $\mathcal{U}$ is the union of horizontal open intervals $(\alpha(y_l), \omega(y_l))$ at level $y = y_l$ (see Figure 2). The type (δ_1, δ_2) of the geometric chirp $\mathcal{U}$ is given in Theorem 3.

Definition 1. *Let $(J_- - J_+)(y,0) < 0$ (resp. > 0), for $y \sim 0$ and $y > 0$, and let $\mathcal{O} = \{y_0, y_1, y_2, \dots\}$ be the orbit with the initial point $y_0 > 0$ defined in (47). The unstable (resp. stable) slow-fast spiral of the contact point of $X_{\epsilon,a,\rho}$, for $(\epsilon, a, \rho) = (0,0,0)$, is the union of the geometric chirp $\mathcal{U}$, defined in (48), and the part of the curve of singularities C between $\alpha(y_0)$ and $\omega(y_1)$ (resp. $\alpha(y_1)$ and $\omega(y_0)$). See Figure 3.*

Remark 5. *Following Definition 1, the stable slow-fast spiral consists of the intervals U_l, pointing from the left to the right, and a part of C. We follow U_0 until we hit C in $x = \omega(y_0)$ (entry). Then we follow the curve C from $x = \omega(y_0)$ to $x = \alpha(y_1)$ (exit), then U_1, the curve C from $x = \omega(y_1)$ (entry) to $x = \alpha(y_2)$ (exit), etc. This way we "spiral" around the origin $(x, y) = (0, 0)$ (and approach the origin). We call this "spiral" the slow-fast spiral because it contains fast and slow intervals of $X_{\epsilon,a,\rho}$ in the limit $\epsilon \to 0$ (thus, the "spiral" is not regular). The unstable slow-fast spiral can be explained in similar fashion.*

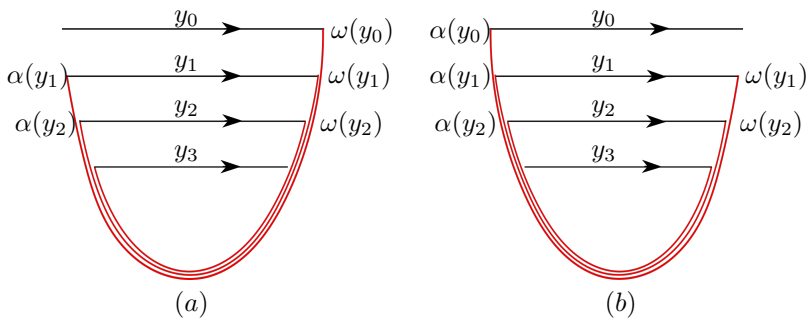

Figure 3: Slow-fast spirals with $x = \omega(y_l)$ as entry and $x = \alpha(y_l)$ as exit for all $l \in \mathbb{N}$. The slow segments are contained in the critical curve C and the slow dynamics along C points from the right to the left. (a) The stable slow-fast spiral. (b) The unstable slow-fast spiral.

Remark 6. *The upper box dimension of the stable or unstable slow-fast spiral from Definition 1 is equal to the upper box dimension of the geometric chirp* $\mathcal{U}$ *defined in (48) because the upper box dimension is finitely stable (see Section 2),* $\dim_B C = 1$ *and* $\overline{\dim}_B \mathcal{U} \geq 1$. *In the rest of this section we therefore focus on the computation of the upper box dimension of* $\mathcal{U}$.

Let denote by $f_i(\rho)$, $i \geq 2n$, the coefficients of the Taylor expansion of F at $x = 0$, i.e. $j^\infty F(x, \rho) = -x^{2n-1} + \sum_{i=2n}^{\infty} f_i(\rho) x^i$. If there exists a nonzero even coefficient $f_{2k}(0)$, we say that $X_{\epsilon,a,\rho}$ has a finite codimension (the smallest $k \geq n$ with this property is the codimension of the contact point in $X_{\epsilon,a,\rho}$). In the generic case ($n = 1$), a similar definition of the codimension can be found in [5].

Theorem 3. *Let* $y_0 > 0$ *be small and fixed and let* $\mathcal{O} = \{y_0, y_1, y_2, \dots\}$ *be the orbit defined by* (47) *tending monotonically to* $y = 0$. *Suppose that the codimension of the contact point in* $X_{\epsilon,a,\rho}$ *is finite and equal to* k. *Then we have* $y_l \simeq l^{-\frac{2n}{2(k-n)+1}}$ *as* $l \to \infty$, $y_l - y_{l+1} \simeq l^{-\frac{2k+1}{2(k-n)+1}}$ *as* $l \to \infty$ *and* $\dim_B \mathcal{O} = \frac{2(k-n)+1}{2k+1} \in (0, 1)$. *Moreover,* $\mathcal{U}$ *is the geometric* (δ_1, δ_2)*-chirp, with* $\delta_1 := \frac{1}{2n}$ *and* $\delta_2 := \frac{2(k-n)+1}{2n}$, *and* $\overline{\dim}_B \mathcal{U} = \frac{4k-2n+1}{2k+1} \in [1, 2)$. *The box dimensions are independent of the initial point* y_0.

Proof. Suppose that the assumptions of Theorem 3 are satisfied. The function $J_- - J_+$, for $\rho = 0$, can be written as

$$(J_- - J_+)(y, 0) = \int_{-y^{\frac{1}{2n}}}^{y^{\frac{1}{2n}}} \frac{4n^2 x^{2n-1} dx}{D(x)} \tag{49}$$

where $y > 0$, $y \sim 0$, $f_i := f_i(0)$, $k \geq n$ is the codimension of $X_{\epsilon,a,\rho}$ ($f_{2k} \neq 0$) and $D(x) = -1 + \sum_{i=n}^{k-1} f_{2i+1} x^{2(i-n+1)} + f_{2k} x^{2(k-n)+1} + O(x^{2(k-n+1)})$. The integrand function in (49) has the following form:

$$\frac{4n^2 x^{2n-1}}{-1 + \sum_{i=n}^{k-1} f_{2i+1} x^{2(i-n+1)}} - 4n^2 f_{2k} x^{2k}(1 + O(x)), \tag{50}$$

where the first term is an odd function. From (49) and (50) follows now that

$$(J_- - J_+)(y, 0) = -\frac{8n^2}{2k+1} f_{2k} y^{\frac{2k+1}{2n}}(1 + o(1)) \tag{51}$$

where $o(1)$ tends to zero when $y \to 0$. In the rest of the proof we assume that $(J_- - J_+)(y, 0) < 0$ for $y \sim 0$ and $y > 0$, i.e. $f_{2k} > 0$ (the case where $(J_- - J_+)(y, 0) > 0$ for $y \sim 0$ and $y > 0$ ($f_{2k} < 0$) can be treated in a similar way). We have

$$\begin{aligned}
(J_- - J_+)(y_l, 0) &= \int_{-y_l^{\frac{1}{2n}}}^{y_l^{\frac{1}{2n}}} \frac{(2nx^{2n-1})^2 dx}{F(x, 0)} \\
&= \int_{-y_l^{\frac{1}{2n}}}^{y_l^{\frac{1}{2n}}} \frac{(2nx^{2n-1})^2 dx}{F(x, 0)} - \int_{-y_l^{\frac{1}{2n}}}^{y_{l+1}^{\frac{1}{2n}}} \frac{(2nx^{2n-1})^2 dx}{F(x, 0)} \\
&= -\int_{y_l^{\frac{1}{2n}}}^{y_{l+1}^{\frac{1}{2n}}} \frac{(2nx^{2n-1})^2 dx}{F(x, 0)} \\
&= \int_{y_l}^{y_{l+1}} 2n(1 + o(1)) du
\end{aligned} \tag{52}$$

where in the second step we use (47) ($\int_{-y_l^{\frac{1}{2n}}}^{y_{l+1}^{\frac{1}{2n}}} = 0$) and in the last step we use the coordinate change $x^{2n} = u$ (the $o(1)$-term in the last integral tends to zero as $u \to 0$). Note that the integrand function in (52) is positive and at least continuous in $u \geq 0$ and $u \sim 0$. Finally, The Mean Value Theorem for Integrals, (51) and (52) imply

$$y_l - y_{l+1} \simeq y_l^{\frac{2k+1}{2n}}, \ l \to \infty. \tag{53}$$

Since $\gamma := \frac{2k+1}{2n} > 1$ ($k \geq n$), Theorem 1 of [6] implies that

$$y_l \simeq l^{-\frac{2n}{2(k-n)+1}}, \ l \to \infty. \tag{54}$$

This together with (53) implies

$$y_l - y_{l+1} \simeq l^{-\frac{2k+1}{2(k-n)+1}},\ l \to \infty.$$

Using Theorem 1 of [6] once more we get

$$\dim_B \mathcal{O} = 1 - \frac{1}{\gamma} = \frac{2(k-n)+1}{2k+1} \in (0,1).$$

The results are clearly independent of the chosen $y_0 > 0$ (see [6]).

It remains to find the upper box dimension of the geometric chirp $\mathcal{U}$. We write $\mathcal{U} = \mathcal{U}_1 \cup \mathcal{U}_2$ where

$$\mathcal{U}_1 = \bigcup_{y_l \in \mathcal{O}} (-y_l^{\frac{1}{2n}}, 0] \times \{y_l\},\ \ \mathcal{U}_2 = \bigcup_{y_l \in \mathcal{O}} [0, y_l^{\frac{1}{2n}}) \times \{y_l\}.$$

From Section 3.6.1 in [22] and (54) follows that $\mathcal{U}_1$ and $\mathcal{U}_2$ are geometric (δ_1, δ_2)-chirps where $\delta_1 := \frac{1}{2n}$ and $\delta_2 := \frac{2(k-n)+1}{2n}$. Now we have (see [22] once more)

$$\overline{\dim}_B \mathcal{U}_1 = \overline{\dim}_B \mathcal{U}_2 = \max\left\{1, 2 - \frac{1+\delta_1}{1+\delta_2}\right\} = \frac{4k-2n+1}{2k+1} \in [1,2).$$

This completes the proof of Theorem 3 since $\overline{\dim}_B \mathcal{U} = \max\left\{\overline{\dim}_B \mathcal{U}_1, \overline{\dim}_B \mathcal{U}_2\right\}$. □

Remark 7. *Let $n \geq 1$ be fixed. Following Theorem 3, there is a one-one correspondence between $\dim_B \mathcal{O}$ (or $\overline{\dim}_B \mathcal{U}$) and the codimension k of the contact point of $X_{\epsilon,a,\rho}$. When $k \to \infty$, then $\dim_B \mathcal{O} \to 1$ and $\overline{\dim}_B \mathcal{U} \to 2$.*

Remark 8. *In [15] it has been proved that $\dim_B \mathcal{O} = \frac{2k-1}{2k+1}$ in the generic case.*

6. Box dimension of 3-dimensional spiral

Using results from [2] for the planar elliptical spiral $\tilde{\Gamma}$

$$\begin{array}{rcl} x(t) & = & t^{-p_0} \cos t \\ y(t) & = & t^{-q_0} \sin t, \end{array} \tag{55}$$

where $0 < p_0 \leq q_0 \leq 1$, we can obtain the box dimension of trajectory of 3-dimensional systems. We formulate this result as an example; a generalization is possible combining the results from [2, 19].

Example 1. *The spiral (55) is the projection of a trajectory of the system*

$$\begin{aligned} \dot{x} &= -y - p_0 x z^{q_0-p_0+1} \\ \dot{y} &= x z^{2(q_0-p_0)} - q_0 y z^{q_0-p_0+1} \\ \dot{z} &= -z^{2+q_0-p_0}, \end{aligned} \tag{56}$$

to the (x, y)-plane. The system (56) is obtained by computing the derivative of (55), using $z = t^{-1}$, and multiplying it by $z^{q_0-p_0} > 0$. The parametrization of the initial curve has been changed, but not the curve itself, so the box dimension of (55) has been preserved, and equal to (see [2])

$$\dim_B \tilde{\Gamma} = 2 - \frac{p_0 + q_0}{1 + q_0}.$$

Using the parametrization

$$\begin{aligned} x(t) &= t^{-p_0} \cos t \\ y(t) &= t^{-q_0} \sin t \\ z(t) &= t^{-1}, \end{aligned} \tag{57}$$

obtained before the time rescaling, we can compute the invariant surface $\frac{x^2}{z^{2p_0}} + \frac{y^2}{z^{2q_0}} = 1$ containing the trajectories of (56). Derivatives $\frac{\partial z}{\partial x}$ and $\frac{\partial z}{\partial y}$ are bounded, so the map $z(x, y)$ is Lipschitz. Using [31] we can conclude that the 3-dimensional trajectory of the system (56) has the same box dimension as the projection curve $\tilde{\Gamma}$.

The projection $\tilde{\Gamma}_{xz}$ of the trajectory of (56) to the (x, z)-plane is a curve called chirp $x(z) = z^{p_0} \cos 1/z$, for $z > 0$ small. We use (see [28])

$$X_{\alpha,\beta}(\tau) = \tau^{\alpha} \sin(\tau^{-\beta}).$$

For $0 < \alpha \leq \beta$ we have

$$\dim_B X_{\alpha,\beta} = 2 - \frac{\alpha + 1}{\beta + 1},$$

and obtain

$$\dim_B \tilde{\Gamma}_{xz} = \frac{3}{2} - \frac{p_0}{2}.$$

Analogously, the projection $\tilde{\Gamma}_{yz}$ of the trajectory of (56) to (y, z)-plane is $y(z) = z^{q_0} \sin 1/z$, with the box dimension

$$\dim_B \tilde{\Gamma}_{yz} = \frac{3}{2} - \frac{q_0}{2}.$$

7. Conclusion

In this paper we have studied the box dimension and Minkowski nondegeneracy/measurability of degenerate spiral trajectories in a class of ordinary differential equations. We give a complete analysis of a polynomial degenerate focus of type (n, n) by connecting it with α-power spirals (see Theorem 1). We also numerically verify this box dimension result. We partially solve the (m, n) case (see Theorem 2) and formulate a conjecture about the box dimension based on numerical experiments. We introduce the notion of slow-fast spiral for planar contact points and find its box dimension (see Theorem 3). We give an example of a 3-dimensional differential equation in presence of an elliptical power spiral as a trajectory.

Acknowledgments

This research was supported by: Croatian Science Foundation (HRZZ) grant PZS-2019-02-3055 from "Research Cooperability" program funded by the European Social Fund.

References

[1] E. Benoit. Équations différentielles: relation entrée–sortie. *C. R. Acad. Sci. Paris Sér. I Math.*, 293(5):293–296, 1981.

[2] S. Burrell, K. Falconer, and J. Fraser. The fractal structure of elliptical polynomial spirals. *preprint (2020)*.

[3] P. De Maesschalck and F. Dumortier. Time analysis and entry-exit relation near planar turning points. *J. Differential Equations*, 215(2):225–267, 2005.

[4] F. Dumortier and R. Roussarie. Canard cycles and center manifolds. *Mem. Amer. Math. Soc.*, 121(577):x+100, 1996. With an appendix by Li Chengzhi.

[5] F. Dumortier and R. Roussarie. Birth of canard cycles. *Discrete Contin. Dyn. Syst. Ser. S*, 2(4):723–781, 2009.

[6] N. Elezović, V. Županović, and D. Žubrinić. Box dimension of trajectories of some discrete dynamical systems. *Chaos Solitons Fractals*, 34(2):244–252, 2007.

[7] K. Falconer. *Fractal Geometry*. John Wiley and Sons, Ltd., Chichester, 1990. Mathematical foundations and applications.

[8] N. Fenichel. Geometric singular perturbation theory for ordinary differential equations. *J. Differential Equations*, 31(1):53–98, 1979.

[9] A. Gasull and J. Torregrosa. A new algorithm for the computation of the Lyapunov constants for some degenerated critical points. In *Proceedings of the Third World Congress of Nonlinear Analysts, Part 7 (Catania, 2000)*, volume 47, pages 4479–4490, 2001.

[10] M. Han and V. G. Romanovski. Limit cycle bifurcations from a nilpotent focus or center of planar systems. *Abstr. Appl. Anal.*, pages Art. ID 720830, 28, 2012.

[11] L. Horvat Dmitrović. Box dimension and bifurcations of one-dimensional discrete dynamical systems. *Discrete Contin. Dyn. Syst.*, 32(4):1287–1307, 2012.

[12] L. Horvat Dmitrović. Box dimension of Neimark-Sacker bifurcation. *J. Difference Equ. Appl.*, 20(7):1033–1054, 2014.

[13] L. Horvat Dmitrović, R. Huzak, D. Vlah, and V. Županović. Fractal analysis of planar nilpotent singularities and numerical applications. *J. Differential Equations*, 293:1–22, 2021.

[14] R. Huzak. Box dimension and cyclicity of canard cycles. *Qual. Theory Dyn. Syst.*, 17(2):475–493, 2018.

[15] R. Huzak, V. Crnković, and D. Vlah. Fractal dimensions and two-dimensional slow-fast systems. *J. Math. Anal. Appl.*, 501(2):Paper No. 125212, 21, 2021.

[16] R. Huzak and D. Rojas. Period function of planar turning points. *Electron. J. Qual. Theory Differ. Equ.*, pages Paper No. 16, 21, 2021.

[17] R. Huzak and D. Vlah. Fractal analysis of canard cycles with two breaking parameters and applications. *Commun. Pure Appl. Anal.*, 18(2):959–975, 2019.

[18] L. Korkut, D. Vlah, D. Žubrinić, and V. Županović. Wavy spirals and their fractal connection with chirps. *Math. Commun.*, 21(2):251–271, 2016.

[19] L. Korkut, D. Vlah, and V. Županović. Geometrical properties of systems with spiral trajectories in $\mathbb{R}^3$. *Electron. J. Differential Equations*, pages No. 276, 19, 2015.

[20] L. Korkut, D. Vlah, and V. Županović. Fractal properties of Bessel functions. *Appl. Math. Comput.*, 283:55–69, 2016.

[21] M. Krupa and P. Szmolyan. Relaxation oscillation and canard explosion. *J. Differential Equations*, 174(2):312–368, 2001.

[22] M. L. Lapidus, G. Radunović, and D. Žubrinić. *Fractal zeta functions and fractal drums*. Springer Monographs in Mathematics. Springer, Cham, 2017. Higher-dimensional theory of complex dimensions.

[23] N. B. Medvedeva. On the analytic solvability of the problem of distinguishing between a center and a focus. *Tr. Mat. Inst. Steklova*, 254(Nelineĭn. Anal. Differ. Uravn.):11–100, 2006.

[24] S. Miličić. Box-counting dimensions of generalised fractal nests. *Chaos Solitons Fractals*, 113:125–134, 2018.

[25] C. Panigrahy, A. Seal, N. K. Mahato, and D. Bhattacharjee. Differential box counting methods for estimating fractal dimension of gray-scale images: a survey. *Chaos Solitons Fractals*, 126:178–202, 2019.

[26] M. Resman. Invariance of the generalized Minkowski content with respect to the ambient space. *Chaos Solitons Fractals*, 57:123–128, 2013.

[27] J.-P. Rolin, D. Vlah, and V. Županović. Oscillatory integrals and fractal dimension. *Bull. Sci. Math.*, 168:Paper No. 102972, 31, 2021.

[28] C. Tricot. *Curves and fractal dimension*. Springer-Verlag, New York, 1995. With a foreword by Michel Mendès France, Translated from the 1993 French original.

[29] D. Žubrinić. Analysis of Minkowski contents of fractal sets and applications. *Real Anal. Exchange*, 31(2):315–354, 2005/06.

[30] D. Žubrinić and V. Županović. Fractal analysis of spiral trajectories of some planar vector fields. *Bull. Sci. Math.*, 129(6):457–485, 2005.

[31] D. Žubrinić and V. Županović. Fractal analysis of spiral trajectories of some vector fields in $\mathbb{R}^3$. *C. R. Math. Acad. Sci. Paris*, 342(12):959–963, 2006.

[32] D. Žubrinić and V. Županović. Poincaré map in fractal analysis of spiral trajectories of planar vector fields. *Bull. Belg. Math. Soc. Simon Stevin*, 15(5, Dynamics in perturbations):947–960, 2008.